Proceedings of the 9th U.S. National and 10th Canadian Conference on Earthquake Engineering
Compte Rendu de la 9ième Conférence Nationale Américaine et
10ième Conférence Canadienne de Génie Parasismique
July 25-29, 2010, Toronto, Ontario, Canada • Paper No 1590

EXPERIMENTAL AND NUMERICAL STUDY ON THE POTENTIAL FOR COLUMN SIZE REDUCTION IN CAPACITY DESIGNED MULTI-STOREY BRACED STEEL FRAMES

C.P. Lamarche[1] and R. Tremblay[2]

ABSTRACT

The 2005 edition of the National Building Code of Canada requires that Concentrically Braced steel Frame (CBF) building structures be designed according to the capacity design principle. In the case of multi-storey CBF building structures, capacity design typically results in larger beam and column sizes compared to traditional design strategies based on the elastic response. This paper aims at presenting results from an experimental and numerical study on the potential for relaxing current capacity design requirements for columns of multi-storey CBF buildings located in seismically active areas. Nonlinear buckling simulation results of an isolated column model were compared to cyclic buckling test results enabling to confirm the adequacy of the Opensees software to model the cyclic nonlinear compressive behaviour of steel columns in the post-buckling range taking into account residual stresses. Exploratory nonlinear seismic dynamic analyses results are presented to show the effects of reducing the size of columns in a two-storey chevron CBF designed according to capacity design principle. From analyses' results, it is demonstrated that it might be possible for CBF building structures with reduced column sizes to sustain temporary dynamic column instability without triggering a global collapse mechanism.

Introduction

In most modern building codes, a capacity design philosophy has been retained for the design of various seismic force resisting systems for which inelastic response is anticipated under design earthquakes. In this approach, components of the seismic force resisting system (SFRS) are designed and detailed to exhibit a ductile response under cyclic inelastic demand. The remaining components, including the columns, must be designed to remain essentially elastic during a strong seismic event. Because the design forces used to select the columns are likely to develop for few short duration peaks during a severe earthquake, current capacity design requirements for the columns have been questioned as it is believed that columns may, under certain conditions, accommodate limited yielding excursions and/or even buckle without adverse significant effects on load carrying capacity.

[1]Assistant Prof., Dept. of Civil Engineering, Université de Sherbrooke, Sherbrooke, PQ, Canada, J1K2R1.
[2]Prof., Dept. of Civil, Mining and Geological Eng., École Polytechnique de Montréal, Mtl, PQ, Canada, H3C3A7.

In this paper, numerical nonlinear buckling simulation results of an isolated column are compared to cyclic buckling test results. The isolated column is modeled using the OpenSees software which has already been proven to reproduce accurately the seismic inelastic cyclic response of steel bracing members (Uriz 2005, Aguero et al. 2006), and the inelastic monotonic buckling behaviour of steel columns including the effect of residual stresses (Lamarche et al. 2008). Finally, exploratory nonlinear seismic analyses results are presented to show the effects of reducing the size of columns in a two-storey chevron braced steel frame (CBF) designed according to capacity design principle. A comparison between the seismic performances of a two storey building designed according to the capacity design principle and the same building with smaller columns is made by use nonlinear dynamic analyses where the intensity of a scaled design ground motion is increase up to global collapse of the structure.

Validation of an isolated column model from experimental data

Buckling test set-up

The column tested was a Class 1 (compact) W310×129 standard steel profile with $L = 3725$ mm and a slenderness ratio $L/r = 48.7$. The steel type was ASTM A992 ($F_y = 345$ MPa). The column test was performed in a 12 MN (2,700 kip) capacity MTS load frame (Fig. 1) in the Hydro-Québec structural research laboratory of École Polytechnique de Montréal. The load frame used can accommodate test specimens as large as 3 m (10'-0") wide and 8.1 m (26'-6") tall. The test specimens were mounted between cylindrical bearings simulating pin-ended boundary conditions for weak-axis buckling and fix-ended conditions for strong-axis buckling at the top and bottom ends. In Figure 1(a), the two 12 MN capacity hardened steel cylindrical hinges with 250 mm radii used to simulate a pinned-pinned condition are also illustrated. The end bearings were designed so that the center of the cylinders coincides with the centroïd of the column cross-sections at the column ends. The instrumentation used during the buckling tests comprised (Fig. 1b&c): 3 potentiometers to measure the out-of-plane displacements at $h/4$, $h/2$, and $3h/4$ (h is the specimen height = 3725 mm), 4 potentiometers, one at each corner of the bottom hinge to measure the axial shortening of the columns, 2 inclinometers to measure the end-rotations, 8 strain gauges positioned at $h/4$ and $h/2$ (total of 16 strain gauges), i.e., one strain gauge on either side (interior and exterior faces) of each of the 4 half flanges positioned at 25 mm from the flanges' tips, and a 12 MN capacity load cell to measure the applied axial force. The test program also comprised four tensile tests performed on coupons taken out of the flanges and web of a virgin piece of W310×129 profile (see Table 1). In Table 1, b is the strain hardening ratio between the kinematic hardening modulus E_{sh} and Young's modulus E. Strain hardening ratio b was determined using an equal plastic energy criteria up to stress F_u. Residual stresses and initial out-of-straightness $\delta_0(x)$ were also measured.

Table 1. Mechanical properties of the steel determined from tensile tests.

	E [GPa]	F_y [MPa]	b [%]
Web	203	350	0.36
Flange	203	371	0.55

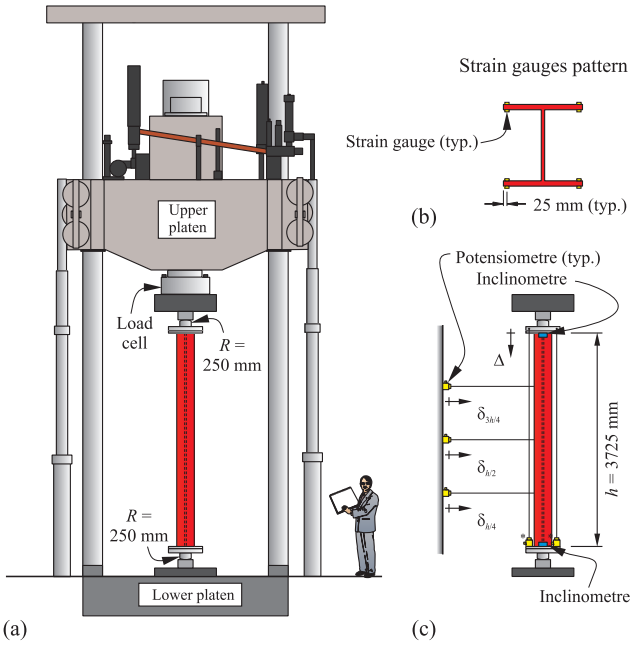

Figure 1. Test set-up: a) testing apparatus, b) strain gauges' pattern at quarter-height and mid-height, c) instrumentation.* Two rows of potentiometers (four in total).

Finite element model of an isolated W310×129 column

The nonlinearBeamColumn finite element of OpenSees was used for the numerical simulation using 8 elements and 5 integration points per element (Fig. 2a). The end conditions were taken as pinned-pinned. The steel material was modeled using the modified Steel02 hysteretic law with residual stress modeling capabilities (Lamarche et al. 2008). The properties of the steel and the Steel02 parameters used for the analysis are summarised in Table 1 and Table 2. A total of 50 fibres were used to discretise the member's cross-section: 20 in each of the two flanges and 10 in the web. The initial out-of-straightness $\delta_0(x)$ and residual stress pattern were taken as those measured experimentally.

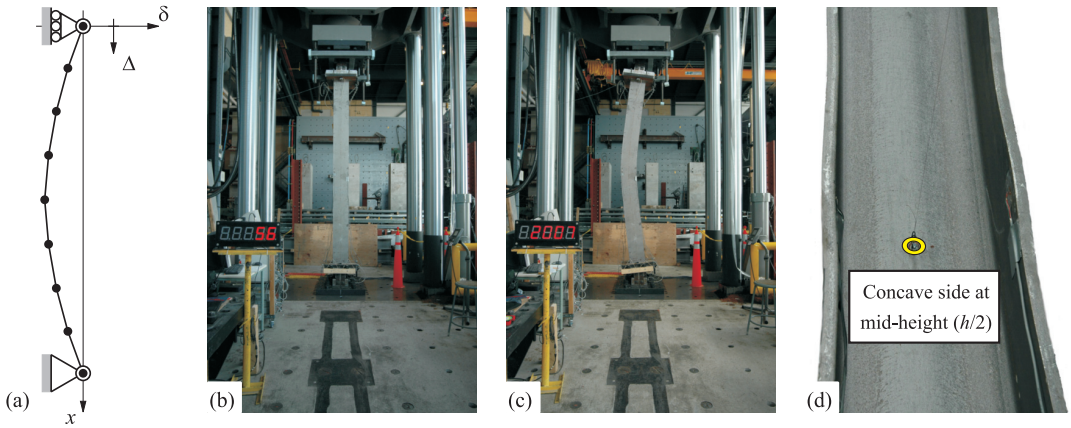

Figure 2. a) Finite element model used for the analysis. Cyclic buckling test: b) prior to the test, c) at the end of the test, d) local buckling at mid-height at the end of the test.

Table 2. Parameters of the Steel02 material used for the analysis.

R_0	cR_1	cR_2	a_1	a_2	a_3	a_4
25	0.925	0.15	0.005	1.0	0.005	1.0

Comparison between the analysis and test results

The cyclic pinned-pinned buckling test performed aimed at verifying the capability of the OpenSees software to accurately model the cyclic inelastic compressive behaviour of steel columns. During the test, an initial 3000 kN static load was initially applied on the column to reproduce the effect of gravity loads. Cyclically applied displacements were then imposed to simulate a seismic demand. Fig. 2b and Fig. 2c present the $L = 3725$ mm W310x129 test specimen before and after the test, respectively. Buckling occurred about the weak axis and local buckling was observed at mi-height at the end of the test, as illustrated in Fig. 2d.

The axial load as a function of the applied axial displacement recorded during the test is compared to the predictions of the OpenSees model with ($\sigma_0 \neq 0$) and without ($\sigma_0 = 0$) the inclusion of initial stresses (Fig. 3a). The ultimate load reached during that test was $C_u = 5399$ kN. The maximum load reached in the OpenSees models with, and without residual stresses are $C_u^{(\sigma 0 \neq 0)} = 5179$ kN , and $C_u^{(\sigma 0 = 0)} = 5624$ kN, corresponding to relative differences of -4.2% and +3.8% respectively. As expected, the maximum load reached including initial stresses in the model is lower than the one where the residual stresses are not accounted for.

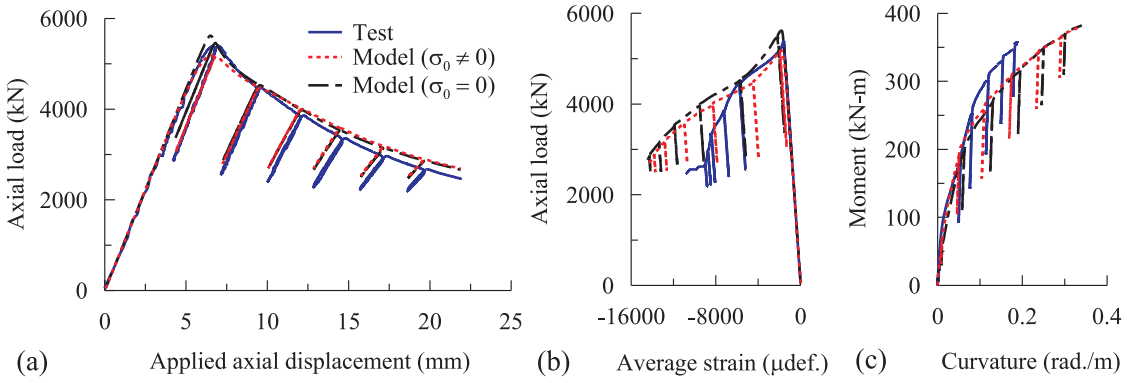

Figure 3. Opensees *vs* test results: a) axial load *vs* applied displacement, b) axial load *vs* average strain at mid-height, c) moment *vs* curvature at mid-height.

In Fig. 3b and 3c, the axial load *vs* average axial strain and curvature plots as obtained from the test and the OpenSees model are compared. When examining the response at mi-height, the results from the numerical model begin to diverge from the measured response at a load of 4300 kN in the post-peak region. This coincides with the initiation of yielding on the convex side of the column and, thereby, beginning of plastic rotation in the plastic hinge at mi-height. The differences can be partly explained by the fact that no imperfections other than initial out-of-straightness in the plane of buckling were included in the finite element model. More importantly, strain-hardening plays a key role in the amplitude of strains in plastic hinge regions, as well as on the length of plastic hinges. Therefore, the properties specified in the model may also have contributed to the divergence of the results in strain at mid-height. Nevertheless,

despite small discrepancies, the global behaviour of the column as modeled with OpenSees is in excellent agreement with the test data. It is clear from Fig. 3a that residual stresses are of greater importance on the prediction of the first buckling load. These effects become less pronounced in the post-buckling range as inelastic axial deformations are applied, which suggests that they may not be critical for prediction of the collapse of structures where the column capacity is exceeded.

Design of the chevron braced steel frame

The chevron CBF used for the analyses was designed according to the latest Canadian seismic provisions, i.e., NBCC 2005 (NRCC, 2005) and CSA-S16S1-05 (CSA-S16, 2005) standards assuming a Type MD (moderately ductile) concentrically braced frame category. A ductility-related force modification factor $R_d = 3.0$ was used in the design. The building is assumed to be located on a site class C in Vancouver, British Columbia. For the design, the bracing members were assumed to be made of ASTM A500 gr. C ($F_y = 345$ MPa) square structural tubing. The cross-section dimensions and wall thicknesses are given in Fig. 4a. ASTM A992 steel ($F_y = 345$ MPa) was adopted for the beams and columns. Fig. 4a shows the geometry of the braced frame studied and the selected steel shapes. The columns are oriented such that the webs are perpendicular to the plane of the frame. Two load cases considered for the design of columns are illustrated in Fig. 4b and Fig. 4c. Case A corresponds to the attainment of the expected buckling capacity of the compression braces at both levels. Case B simulates the post-buckling situation of the compression braces and yielding of the tension braces. The resulting axial loads in the most heavily loaded column in compression (bottom floor column on the right-hand side in the figure) are respectively equal to 1340 kN and 2136 kN. The latter value was used for the selection of the W250×80 shape. A W250×58 column would have been needed had only Case A been considered in design.

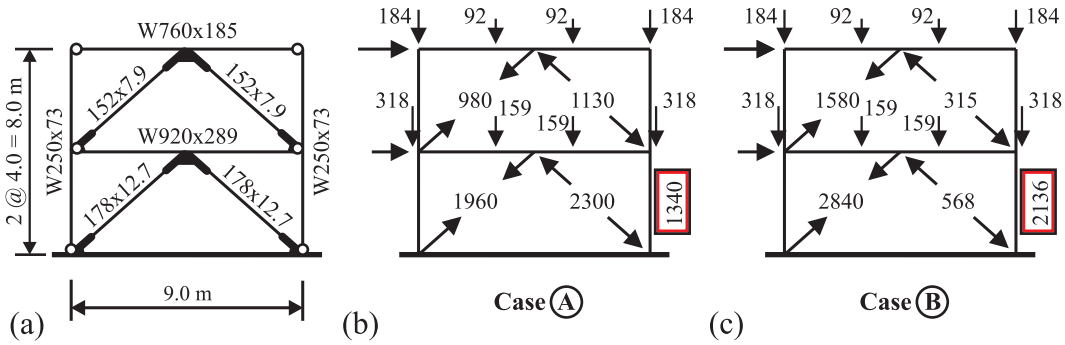

Figure 4. Two-storey chevron braced frame: a) geometry, b) design loads at brace buckling, and c) design loads after brace buckling (forces in kN).

Nonlinear dynamic analyses

The columns were modeled using 8 nonlinearBeamColumn OpenSees elements per member with 5 integration points per element. As in the isolated column case, 50 fibres were used to discretise the member's cross-section. The bracing members were modeled using 8 elements with 4 integration points per element. The cross-section was discretised using 20 fibres (Aguerro et al. 2006) and an initial out-of-straightness $\delta_0 = L/300$ was considered to obtain

compression strength consistent with design assumptions. The dimensions as well as the rotational stiffness and strength of the gusset plates were also modeled using rigid extensions and nonlinear rotational springs. The beams were modeled using 6 nonlinearBeamColumn elements with 4 integration points per element and 50 fibres per section. Beam-to-column connections and column bases were assumed to be pinned. Initial frame out-of-plumb was ignored in the design and the analyses. In the analyses, an expected steel yield strength $R_y F_y = 380$ MPa was adopted for all members. Half-sine wave initial column out-of-straightness was assumed with maximum amplitude $\delta_0 = L/1000$ at column mid-height. The residual stress pattern proposed by Galambos & Ketter (1959) and used recently by Surovek-Maleck & White (2004) was adopted:.

$$\sigma_t = \left(\frac{bt}{bt + w(d - 2t)} \right) \sigma_c \qquad (1)$$

where b and t are the flange width and thickness, respectively, d is the beam depth and w is the web thickness, and σ_c and σ_t are the compression and tension stresses at the flange tip and middle of flange, respectively. In this study, σ_c was taken equal to 0.3 F_y. The first two natural vibration periods of the building for both design cases were: $T_1 = 0.416$ s and $T_2 = 0.0595$ s for design Case A, and $T_1 = 0.413$ s and $T_2 = 0.0595$ s for design Case B. The response of the braced frame was examined under 0.8 times the Castaic, Old Ridge Rd. 90° motion recorded during the M6.7 Jan. 17, 1994 Northridge earthquake. Fig. 5a shows the first 15 seconds of the scaled horizontal ground acceleration record. The corresponding pseudo-acceleration spectrum S_a is compared to the NBCC 05 design spectrum in Fig. 5b. Nonlinear dynamic analyses of the structure were performed using the implicit Newmark average acceleration integration scheme with Newton iteration to reach convergence using $\Delta t = 0.005$ s. Rayleigh damping corresponding to 3% of critical damping in the first two modes of vibration was specified in the analyses. The structure with reduced column size was designed assuming that only load Case A of Fig. 4 would have been considered in design. W250×58 columns were chosen for that particular case.

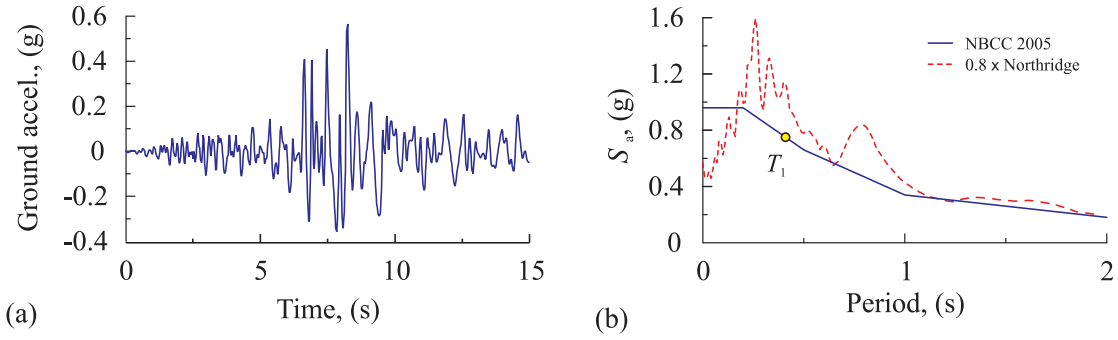

Figure 5. Selected 1994 Northridge earthquake record: a) time history, b) pseudo-acceleration spectrum and NBCC 2005 design spectrum.

Seismic performance of the chevron CBF using columns with reduced capacity

The seismic performance of the chevron CBF designed according to Case A and Case B of Fig. 4, i.e., the reduced column case and the full capacity design (CD) case, were investigated. The structures were submitted to increasing levels of the scaled Northridge earthquake record.

For both structures, the expected maximum base shear assuming that the tension and compression braces at the base floor reach their expected strengths simultaneously is $V_{\max}^{(e)} = 3184$ kN. Fig. 6a and Fig. 6b present the storey shear contributed by each bracing member as well as the total storey shear at both levels for design Case A. All values are normalized with respect to $V_{\max}^{(e)}$. In Fig. 6a, the base shear is in excellent agreement with the expected maximum base shear $V_{\max}^{(e)}$. A plot relating the normalized peak base shear $V_{\max}/V_{\max}^{(e)}$ to the design earthquake multiplier (EQ_M) for each building structure is presented in Fig. 6c. In the figure, $EQ_M = 1.0$ correspond to the Northridge record scaled to the design level, i.e., 0.8 times the Northridge record (Fig. 5). In Fig. 6c, in the $1.0 \le EQ_M \le 1.5$ range, $V_{\max}/V_{\max}^{(e)} \approx 1.0$, which confirms the adequateness of the numerical bracing models as well as the adequateness of the scaling factor used. Above $EQ_M = 1.5$, the peak base shear ratio slowly increases above unity as strain hardening of the steel in the bracing members becomes more important due to the increased lateral ductility demand. The varation of the lateral ductility at each storey with EQ_M is illustrated in Fig. 7a. The ductility is defined as the peak storey drift divided by the storey drift inducing buckling of the compression brace. The ductility of the two structures in Fig. 7a is similar at each storey up to $EQ_M = 0.75$. Beyond this value and up to $EQ_M = 1.1$, there is concentration of ductility at the first level of Case A frame and at the second storey for the capacity designed structure. Above $EQ_M = 1.1$, the ductility response for both design cases regroups until collapse of the Case A structure at $EQ_M = 1.45$. The global lateral ductility based on roof drift is presented in Fig. 7b for both structures. As assumed in design, both structures remain in the linear regime up to the point $EQ_M = 1/R_d = 0.33$, and a ductility of 3.0 ($= R_d$) is reached at approximately $EQ_M = 1.0$. For design Case A, sudden collapse occurs at $EQ_M = 1.35$ at a global ductility of 4.5. For the full capacity design case, collapse is more gradual and is initiated at $EQ_M = 1.5$, at a global ductility of 5.5.

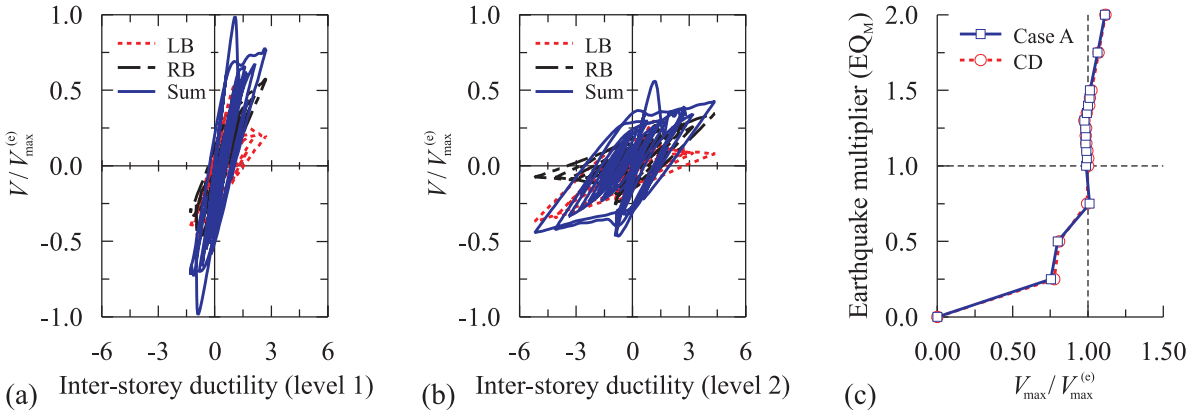

Figure 6. Normalised peak shear at: a) storey 1, b) storey 2, and c) earthquake multiplier (EQ_M) *vs* normalised base shear. (LB: left brace, RB: right brace)

The axial load demand on the bottom storey portion of the left and right hand side columns of the Case A structure are presented in Fig. 8 for $1.0 \le EQ_M \le 2.0$. In the figure, the peak compressive loads $C_{\max}$ are normalised with respect to the expected compressive strength, C_u, of the column W250x58. The strength C_u is defined as $C_u = C_r R_y/\phi = 1589$ kN, with $R_y = 1.1$,

$\phi = 0.9$ and the factored resistance, $C_r = 1301$ kN. The ratio C_{res}/C_u is also plotted in the figure, where C_{res}, is the column residual compressive strength, defined as the lowest post-buckling resistance reached by the column during the analysis. When column buckling does not occur during an analysis, C_{res} is set equal $C_{res} = \max(C_u; C_{max})$. In Fig. 8, buckling has occurred if $C_{res} < C_{max}$, i.e., the column buckled at a load C_{max} and its capacity subsequently reduced to C_{res}. Buckling was first encountered on the left hand side at $EQ_M = 1.05$. In the $1.1 \le EQ_M \le 1.35$ range, the left-hand side column buckled without triggering the global collapse of the structure. In that particular case, the building could thus safely sustain a 35% increase of the design earthquake level even if column buckling had occurred. The right-hand side column did not buckle until EQ_M reached 1.5. For design case CD (not shown), no column buckling was observed, as expected.

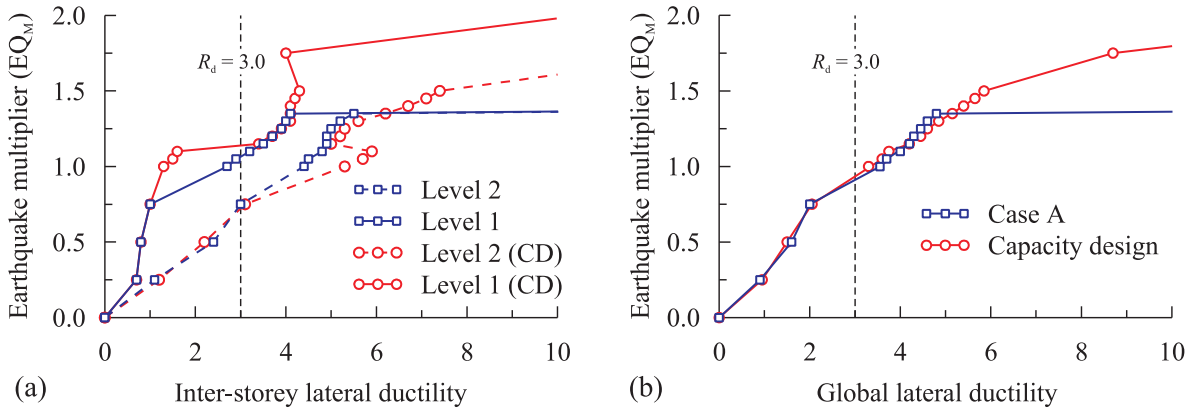

Figure 7. Lateral horizontal ductility demand: a) bottom and top storeys, b) global ductility.

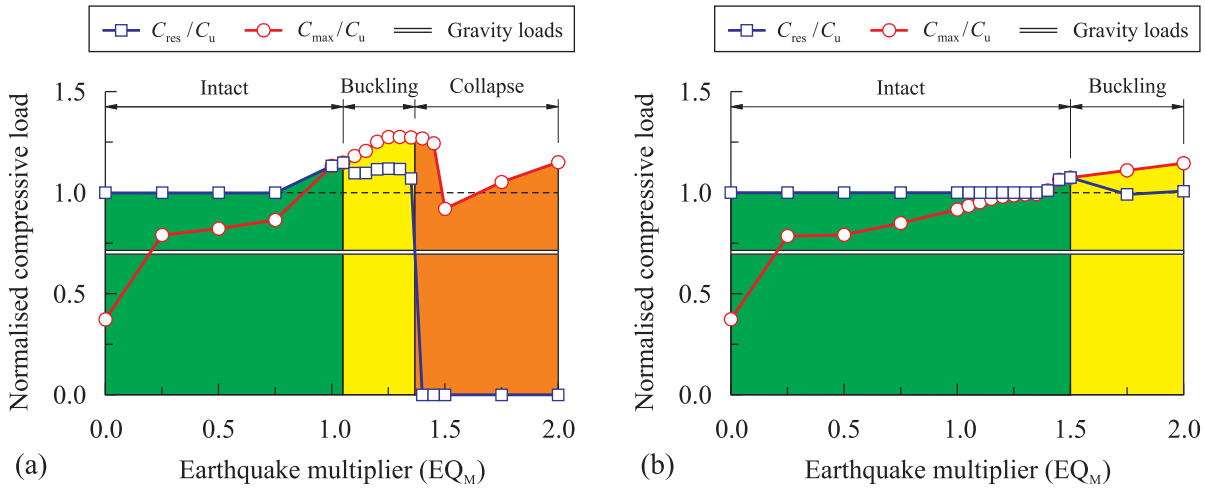

Figure 8. Normalised compressive load *vs* EQ_M curves: a) left column, b) right column.

In Fig. 8, the left- and right-hand side columns were capable of carrying axial load C_{max} that were up to 20% and 10% larger, respectively, than the column expected buckling strength C_u. This apparent inconsistency is attributed to the fact that the column was made of a single member continuous over the two storeys. The upper column segment carrying lower load could

then provide restraint to the bottom storey segment and increase its buckling strength beyond the capacity based on pinned-pinned condition. Fig. 9a shows the axial load *vs* axial deformation response of a pinned-pinned W250×58 column with $L = 4000$ mm taking into account residual stress and initial out-of-straightness, as obtained from Opensee simulation. The so-obtained buckling load $C_u^{(p)} = 1574$ kN, which corresponds to 99% of the expected load $C_u = 1589$ kN. Fig. 9a also presents pinned-pinned model simulation responses of a two-storey ($L = 8000$ mm) W250×58 column with same residual stress and initial out-of-straightness conditions. For that column, the gravity loads P_D at the first and second storey of the building studied were applied first and the vertical loads induced by the braces upon increasing the lateral seismic loads (ηP_E) were gradually applied at each level (Figs. 9b&c). This was done for loading Cases A and B and it is shown in Fig. 9a that the column can carry axial loads in excess of C_u under these conditions. Column buckling in these two-storey simulations occurred at $1.18C_u$ and $1.16C_u$ for load Cases A and B, respectively, which is comparable to the response of the left-hand side column of the structure studied in the incremental analysis, as illustrated in Fig. 9d. In Figs. 9a&c, Case C is a simulation where the total load is applied at the roof level. In that case, the column buckles close to the load C_u, as expected. These simulations clearly show that column continuity in multi-storey structures can result in increased column buckling strength.

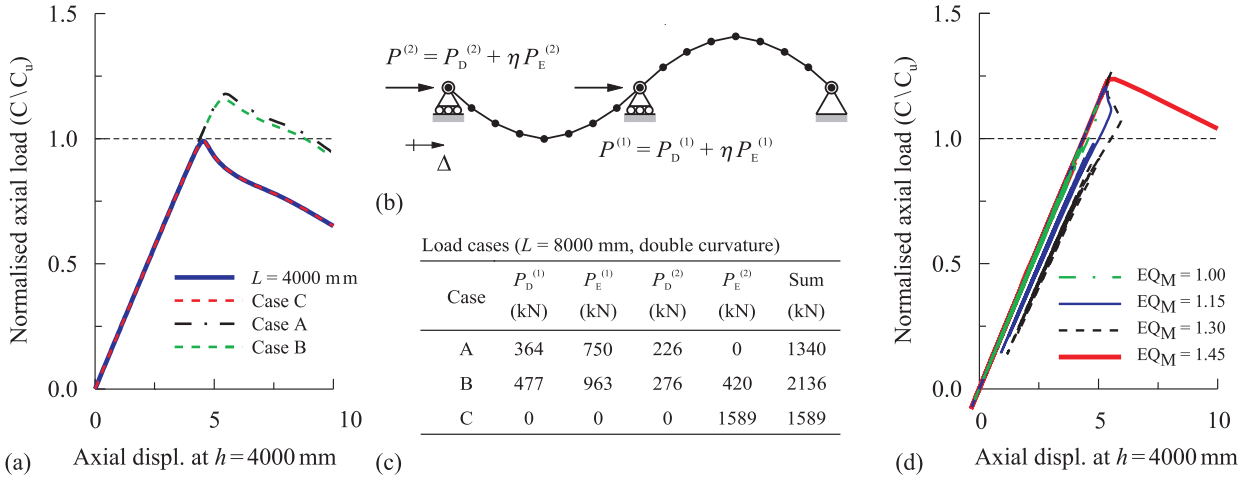

Load cases (L = 8000 mm, double curvature)

Case	$P_D^{(1)}$ (kN)	$P_E^{(1)}$ (kN)	$P_D^{(2)}$ (kN)	$P_E^{(2)}$ (kN)	Sum (kN)
A	364	750	226	0	1340
B	477	963	276	420	2136
C	0	0	0	1589	1589

Figure 9. a) Normalised buckling curves for various load cases, b) model in double curvature and applied load pattern, c) load cases investigated, d) behaviour of the left bottom-storey column for various EQ_M values.

Conclusions

Numerical nonlinear buckling simulation results of an isolated column model were compared to cyclic buckling test results. The numerical simulation confirmed the adequacy of the Opensees software to model the cyclic nonlinear compressive behaviour of steel columns in the post-buckling range taking into account residual stresses and initial out-of-straightness. Exploratory incremental nonlinear seismic analyses were performed to study the effects of reducing the size of columns in a two-storey chevron CBF designed according to capacity design principle. In all analyses, the numerical models were carefully calibrated and validated such that the ultimate loads carried by the elements were in accordance with the expected capacity used in

design. Up to collapse, the structure with the reduced columns exhibited a seismic response comparable to that of the structure complying with current code capacity design rules. Collapse of the frame with reduced columns occurred earlier and in a sudden manner, as a result of the column compressive strength in the post-buckling range reducing below the applied gravity load level. No column instability occurred in the structure designed according to capacity design principle, and progressive collapse due to excessive storey drifts was observed. The study showed however that CBFs with reduced column sizes can sustain, without global structural collapse, temporary column instability under dynamic seismic loading. Column compressive overstrength was also found to be present in continuous columns used in multi-storey structures. Additional study should be conducted to further study this response. The possible effects of seismic induced dynamic strain rates on column buckling should be examined in future studies.

Acknowledgments

The financial support from the Fonds québécois de la recherche sur la nature et les technologies (FQRNT) of the Government of Quebec, Canada, and from the Natural Sciences and Engineering Research Council of Canada (Canada Research Chair program) is acknowledged. Denis Fortier, Patrice Bélanger, Viacheslav Koval, David Ek, Marc Charbonneau, and Eddy Saavedra at the Hydro-Québec structural research Laboratory at École Polytechnique de Montréal are also acknowledged for their invaluable assistance. The help of the undergraduate students working part-time at the laboratory is also acknowledged.

References

Agüero, A., Izvernari, C., and Tremblay, R., 2006. Modelling of the Seismic Response of Concentrically Braced Steel Frames using the OpenSees Analysis Environment. *International Journal of Advanced Steel Construction*, 2(3), 242–274.

Canadian Standards Association (CSA), 2005. Limits states design of steel construction, including CSA-S16S1-05 supplement no. 1. Mississauga, ON, CAN/CSA-S16.1.

Galambos, T.V., Ketter, R.L., 1959. Columns under combined bending and thrust. *Journal of the Engineering Mechanical Divivision* (ASCE), 85, 1–30.

Lamarche, C.P, Tremblay, R., 2008. Accounting for residual stresses in the seismic stability of nonlinear beam-columns elements with cross-section fibre discretization. Structural Stability Research Council (SSRC) - Proceedings of the 2008 Annual Stability Conference, (pp. 59-78). Nashville.

National Research Council of Canada (NRCC), 2005. National Building Code of Canada (NBCC), 12th ed., Ottawa, ON.

Surovek-Maleck, A. & White, D.W., 2004. Alternative approaches for elastic analysis and design of steel frames. I: Overview. *Journal of Structural Engineering (ASCE)*, 130(8), 1186–1196.

Uriz, P., 2005. Towards Earthquake Resistant Design of Concentrically Braced Steel Structures. Ph.D. Thesis. Dept. of Civ. Eng., University of California, Berkeley, CA.